JBC RESEARCH ARTICLE

In vitro reconstitution of Sgk3 activation by phosphatidylinositol 3-phosphate

Received for publication, April 16, 2021, and in revised form, June 9, 2021 Published, Papers in Press, June 25, 2021,
https://doi.org/10.1016/j.jbc.2021.100919

Daniel Pokorny[1,2], **Linda Truebestein**[1,2], **Kaelin D. Fleming**[3], **John E. Burke**[3,4], **and Thomas A. Leonard**[1,2,*]

From the [1]*Department of Structural and Computational Biology, Max Perutz Labs, Vienna, Austria;* [2]*Department of Medical Biochemistry, Medical University of Vienna, Vienna, Austria;* [3]*Department of Biochemistry and Microbiology, University of Victoria, Victoria, British Columbia, Canada; and* [4]*Department of Biochemistry and Molecular Biology, The University of British Columbia, Vancouver, British Columbia, Canada*

Edited by Dennis Voelker

Serum- and glucocorticoid-regulated kinase 3 (Sgk3) is a serine/threonine protein kinase activated by the phospholipid phosphatidylinositol 3-phosphate (PI3P) downstream of growth factor signaling *via* class I phosphatidylinositol 3-kinase (PI3K) signaling and by class III PI3K/Vps34-mediated PI3P production on endosomes. Upregulation of Sgk3 activity has recently been linked to a number of human cancers; however, the precise mechanism of activation of Sgk3 is unknown. Here, we use a wide range of cell biological, biochemical, and biophysical techniques, including hydrogen–deuterium exchange mass spectrometry, to investigate the mechanism of activation of Sgk3 by PI3P. We show that Sgk3 is regulated by a combination of phosphorylation and allosteric activation. We demonstrate that binding of Sgk3 to PI3P *via* its regulatory phox homology (PX) domain induces large conformational changes in Sgk3 associated with its activation and that the PI3P-binding pocket of the PX domain of Sgk3 is sequestered in its inactive conformation. Finally, we reconstitute Sgk3 activation *via* Vps34-mediated PI3P synthesis on phosphatidylinositol liposomes *in vitro*. In addition to identifying the mechanism of Sgk3 activation by PI3P, our findings open up potential therapeutic avenues in allosteric inhibitor development to target Sgk3 in cancer.

Cellular membranes are hotspots at which numerous signaling pathways controlling various aspects of cell physiology and pathology converge. One of the most intensively studied pathways downstream of extracellular growth factors is the phosphoinositide 3-kinase (PI3K) pathway. PI3K activation by receptor tyrosine kinases, G-protein-coupled receptors, or RAS leads to the generation of various phosphoinositide lipids that serve as a platform for the recruitment and activation of effector molecules (1). Dysregulation of PI3K signaling is frequently observed in cancer, diabetes, neurodegenerative and cardiac disorders, and other diseases (2, 3), making the pathway a prominent target for pharmacological inhibition (4).

Many important downstream effectors of PI3K are protein kinases. Protein phosphorylation is a ubiquitous post-translational modification that regulates cell signaling and is carried out by the arsenal of more than 500 protein kinases in the human proteome (5). Since the mechanism of phosphotransfer catalyzed by protein kinases is highly conserved (6), individual kinases have evolved unique regulatory mechanisms to ensure that they can faithfully respond to different, often very transient, lipid-based signaling cues (7).

Serum- and glucocorticoid-regulated kinase 3 (Sgk3) (also known as cytokine-independent survival kinase [CISK]) is a serine/threonine protein kinase that is activated downstream of growth factors (8). Like the closely related kinase Akt, it belongs to the AGC kinase family and is activated by phosphorylation of a hydrophobic motif in its C-terminal tail by mTORC2 (9) and subsequent PDK1-dependent phosphorylation of its activation loop (10, 11). A third site, called the turn motif, also in the tail, regulates the stability of Akt and protein kinase C (PKC) (12, 13), but its phosphorylation has not been reported in Sgk3. Distinct from the activation of Akt by phosphatidylinositol-3,4,5-trisphosphate (PIP_3) or phosphatidylinositol-3,4-bisphosphate [$PI(3,4)P_2$], Sgk3 depends on the lipid PI3P for its activation (14). Sgk3 is recruited specifically to endosomes *via* its PI3P-binding phox homology (PX) domain (15, 16), which promotes phosphorylation of its activation loop and hydrophobic motif by PDK1 and mTORC2, respectively (9, 15, 17). Two major pathways drive the production of PI3P on endosomes. Downstream of PIP_3 production by class I PI3K at the plasma membrane, $PI(3,4)P_2$ is produced by the action of SH2-containing inositol 5′ phosphatase (SHIP2) (18, 19). Phosphatidylinositol-3-phosphate (PI3P) is generated either from $PI(3,4)P_2$ by inositol polyphosphate 4-phosphatases (INPP4) (20) or, *de novo*, from phosphatidylinositol by the class III PI3K Vps34 (21). Both pathways have been shown to contribute to Sgk3 activation (17, 22). Loss of heterozygosity in INPP4B, which leads to the upregulation of PI3K signaling, has been reported in a majority of basal-like breast cancers and a significant proportion of ovarian cancers (23).

Sgk isoforms are transcriptionally induced by serum and glucocorticoid hormones (24) and are involved, among others,

* For correspondence: Thomas A. Leonard, thomas.leonard@meduniwien.ac.at.

in the regulation of ion channels, transcription factors, enzymatic activities, and have been implicated in hair growth defects and renal dysfunction (25). Recently, Sgk3 has been shown to play a role in different cancers in an Akt-independent manner (9, 26–28), highlighting the importance of Sgk3 as an effector downstream of PI3K signaling. Despite its physiological and pathological relevance, however, relatively little is known about the precise mechanism of Sgk3 regulation. In this manuscript, we provide clear evidence for the allosteric activation of Sgk3 by PI3P, highlighting the role of the PX domain and PI3P in the regulation of Sgk3 enzymatic activity. Our findings have obvious implications for the spatial and temporal control of Sgk3 activity as well as for the design of Sgk3-targeted therapeutics.

Results

Sgk3 localizes specifically to PI3P-containing endosomes

The Sgk3 PX domain (residues 1–124) has previously been shown to bind to PI3P and is required for localization at early endosomes (14, 17, 29, 30). Serum-starved HeLa cells transfected with mCherry-Sgk3 show a punctate endosomal membrane localization (Fig. 1*A*), which is lost upon 20 min treatment with the PI3K inhibitor wortmannin (Fig. 1*B*). The membrane localization of Sgk3 is strictly dependent on its PX domain, since a binding site mutant of Sgk3 ($Sgk3^{R90A}$) fails to localize to endosomes in the same cells (Fig. 1, *C* and *D*). This is further illustrated by a representative cross section intensity profile (Fig. 1, *E* and *F*). To confirm that Sgk3 localizes specifically to endosomes, we cotransfected HeLa cells with eGFP-tagged FYVE domain from early endosomal antigen 1 (EEA1), which is a marker of early endosomes and has previously been used to assess Sgk3 localization (17). Figure 1, *G–J* show that Sgk3 colocalizes with punctae positive for $EEA1^{FYVE}$. Together, these data confirm both the specificity of Sgk3 for PI3P and the localization of Sgk3 to endosomes.

In vitro *characterization of recombinant Sgk3*

Expression of Sgk3 as an N-terminal eGFP fusion protein led to approximately 2–3 orders of magnitude increased yields. Proteolytic cleavage of the fusion protein to remove the eGFP yielded monodisperse and pure, monomeric Sgk3

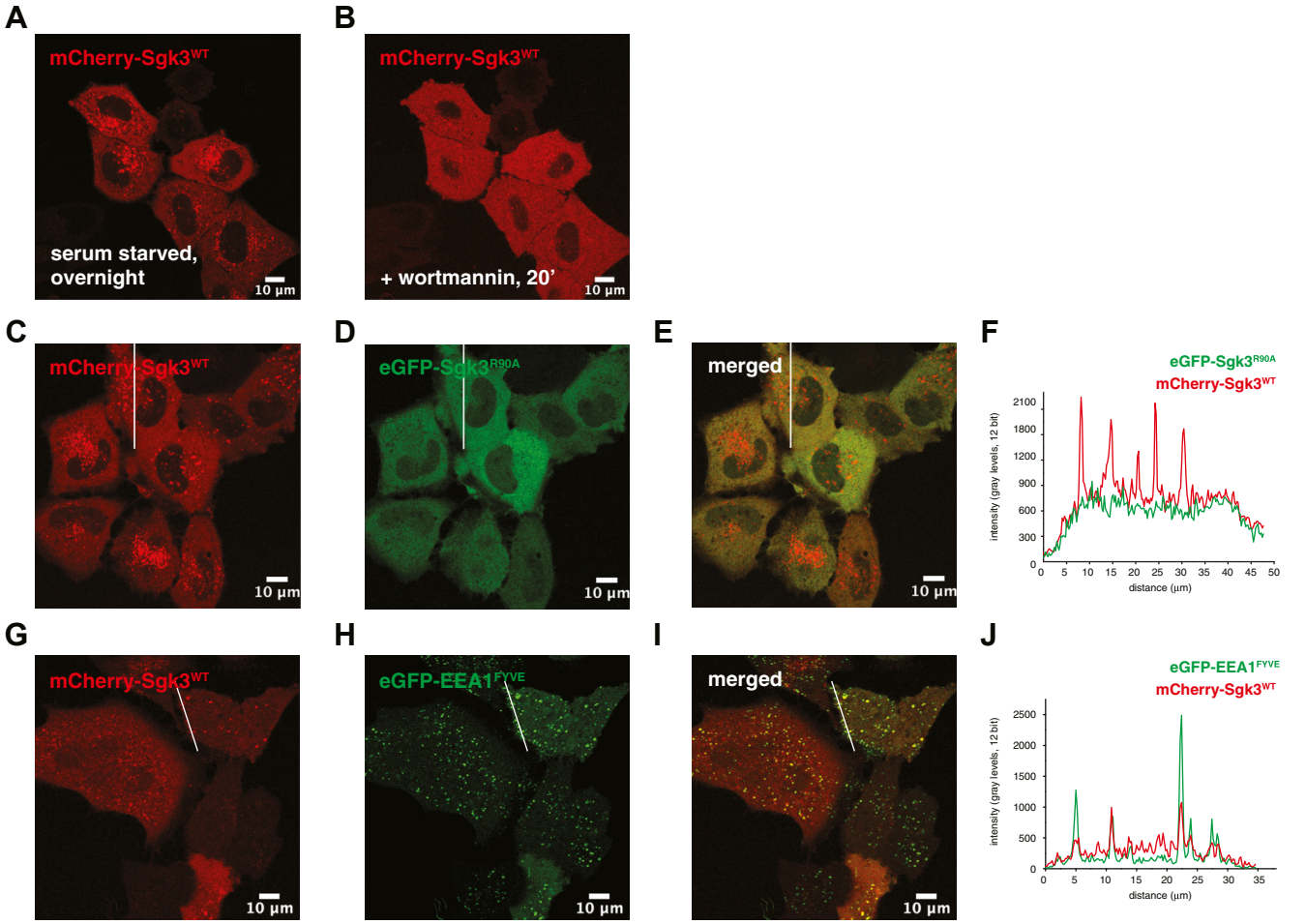

Figure 1. Sgk3 localizes specifically to PI3P-containing endosomes. All images are representative of three independent transfections and multiple fields of view. *A*, HeLa cells were transfected with mCherry-$Sgk3^{WT}$ and serum-starved overnight. *B*, starved cells were treated with 100 nM wortmannin for 20 min. *C–E*, cells were cotransfected with mCherry-$Sgk3^{WT}$ and eGFP-$Sgk3^{R90A}$ mutant. *F*, fluorescence intensity profile of mCherry $Sgk3^{WT}$ and eGFP-$Sgk3^{R90A}$ along the white line shown in *C–E*. *G–I*, cells were cotransfected with mCherry-$Sgk3^{WT}$ and eGFP-$EEA1^{FYVE}$. *J*, fluorescence intensity profile of mCherry $Sgk3^{WT}$ and eGFP-$EEA1^{FYVE}$ along the white line shown in *G–I*.

(Fig. S1, *A* and *B*). The phosphorylation state of recombinant human Sgk3 co-expressed with PDK1 and purified from baculovirus-infected insect cells was characterized by tandem mass spectrometry (Fig. S1*C*). Sub-stoichiometric (∼20%) activation loop (Thr320) phosphorylation was observed; however, phosphorylated peptides were not observed for either the turn motif (Ser461) or the hydrophobic motif (Ser486), despite purification with phosphatase inhibitors known to preserve phosphorylation at these sites in Akt1. Turn motif phosphorylation has previously been reported for Sgk1 (31) and other AGC kinases, in particular Akt and PKC, in which it plays an important role in regulating protein stability and degradation (12, 13, 32, 33). Since both the turn motif and the basic patch to which it binds on the kinase domain are conserved, it seemed logical to assume that Sgk3 should also be modified at this site. Insects, however, do not express an obvious homolog of Sgk3, raising the possibility that the kinase responsible for turn motif phosphorylation of Sgk3 is also not present in insect cells. We therefore expressed human Sgk3 in HEK293T cells and characterized its phosphorylation state by tandem mass spectrometry. Surprisingly, phosphorylated peptides were again not observed for either the turn motif or hydrophobic motif (Fig. S1*D*). It is therefore an open question as to whether Sgk3 is indeed modified on the turn motif and under what cellular conditions.

To prepare site-specifically phosphorylated Sgk3 for *in vitro* kinase assays, both wild-type Sgk3 ($Sgk3^{WT}$) and kinase-dead Sgk3 ($Sgk3^{D286A}$) were dephosphorylated with lambda phosphatase and re-phosphorylated with recombinant PDK1. Specific modification of Sgk3 with a single phosphate on its activation loop (Thr320) was confirmed by mass spectrometry (Fig. S1, *E* and *F*). The purification of recombinant Sgk3 was challenging, due to solubility issues under certain purification conditions. However, careful optimization of the purification protocol enabled us to purify Sgk3 in a detergent-free buffer with pH and ionic strength close to physiological values (see Experimental Procedures). We performed size-exclusion chromatography coupled to multi-angle light scattering to determine its precise mass and monodispersity. Sgk3 exhibited a single peak with a measured mass of 57.3 kDa, in close agreement with its actual mass reported by mass spectrometry and a polydispersity value of 1.001 (Fig. S1*G*). To ensure that the Sgk3 used in subsequent assays was monodisperse and remained so for the duration of the assays, we measured the particle size distribution of Sgk3 by dynamic light scattering at 0 and 60 min post-freeze–thaw under kinase assay buffer conditions. Sgk3 exhibited near identical mass distributions centered on a particle size of 3 nm at 0 and 60 min at 20 °C (Fig. S1*H*).

Sgk3 is specifically and allosterically activated by PI3P

Previous studies have shown that loss of PI3P binding decreases phosphorylation of Sgk3 on its activation loop and hydrophobic motif (15), as well as downstream substrate phosphorylation (9). However, it is not known whether PI3P binding serves to allosterically activate Sgk3 in addition to its known role in promoting phosphorylation of the activation loop and hydrophobic motif (17). Previous studies have established that the closely related kinase Akt depends on the binding of $PI(3,4,5)P_3$ or $PI(3,4)P_2$ for full activity (34, 35). We therefore investigated whether PI3P is simply a membrane anchor to target Sgk3 to endosomes or whether PI3P also allosterically governs Sgk3 activity.

Having established that our recombinant Sgk3 is well behaved during our assays, we assessed the influence of PI3P on kinase activity. Dephosphorylated Sgk3 exhibited undetectable kinase activity *in vitro* and could not be stimulated with PI3P (Fig. S2*A*). To test whether PI3P allosterically activates Sgk3, we bound PDK1-phosphorylated $Sgk3^{WT}$ to liposomes with increasing PI3P concentrations and assayed its kinase activity against Crosstide, a glycogen synthase kinase 3β (GSK3β)-derived peptide substrate of Sgk3 (36), using a radiometric kinase assay (37). We observed robust, PI3P-dependent activation of Sgk3, which correlated with the fraction of protein bound to the liposomes (Fig. 2*A*). Both the activity and binding curves can be fitted with a one-site binding model characterized by nearly identical binding affinities of 24.6 ± 10.8 μM and 29.3 ± 8.0 μM, respectively. No signal was observed in the control without Crosstide, thereby ruling out autophosphorylation of Sgk3. Basal kinase activity against Crosstide seen in the absence of PI3P can be explained by the high degree of activation loop phosphorylation (Fig. S1*E*). To confirm that the observed activity comes exclusively from Sgk3, we mutated D286 in the catalytic loop to alanine to create a kinase-dead Sgk3. While this protein shows almost identical PI3P binding to $Sgk3^{WT}$, neither basal nor PI3P-stimulated Crosstide phosphorylation was observed (Fig. 2*B*).

We next reconstituted Sgk3 activation by PI3P *in vitro* using a coupled Vps34-Sgk3 kinase activity assay. Vps34 is the only class III PI3K expressed in mammalian cells and generates PI3P from PI on endosomes and other endomembrane structures, including autophagosomes (38, 39). We prepared liposomes containing 10 mol % PI as a substrate for Vps34 and monitored both Vps34 and Sgk3 activity simultaneously in a radiometric kinase assay (Fig. 2*C*). We could detect a time-dependent production of PI3P in the liposomes and the consequent binding and activation of Sgk3 as a function of increasing PI3P (Fig. 2*D*). The phosphorylation of Crosstide can be fully attributed to Sgk3, as a control experiment in the absence of Sgk3 exhibited no phosphorylation (Fig. S2*B*). This demonstrates that Sgk3 is allosterically activated by the product of class III PI3K activity, highlighting that full Sgk3 activity requires membranes enriched in PI3P.

HDX-MS reveals conformational changes in Sgk3 upon membrane binding

Having demonstrated that Sgk3 is allosterically activated by PI3P, we next set out to investigate the structural basis of PI3P-mediated activation. In previous studies on Akt, we have

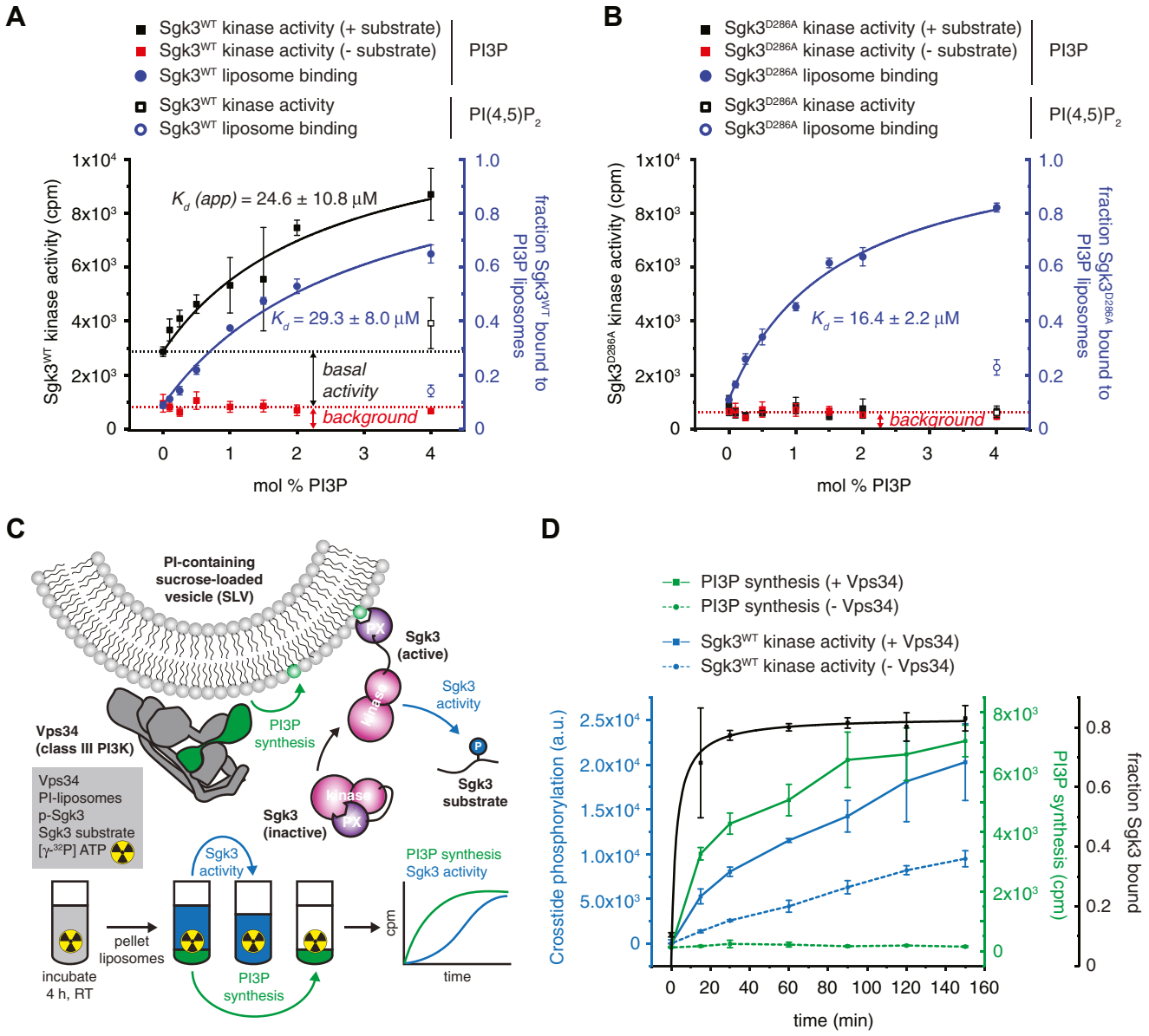

Figure 2. Sgk3 is specifically and allosterically activated by PI3P. *A*, Sgk3^{WT} kinase activity was assayed in the presence (*closed black square*) or absence (*closed red square*) of 100 µM Crosstide substrate with 0–4 mol % PI3P liposomes or with 4 mol % PI(4,5)P_2 liposomes (*open black square*) as a negative control. In parallel, binding of Sgk3 to 0–4 % PI3P liposomes (*full blue circles*) or 4% PI(4,5)P_2 (*open blue circle*) as a negative control was measured. *Dotted black line* indicates basal Sgk3^{WT} kinase activity of unbound protein, *dotted red line* indicates no-substrate control. Kinase activity was read out radiometrically by liquid scintillation and liposome binding by Coomassie densitometry. Error bars are the standard deviation of three independent experiments. *B*, same as (*A*) with Sgk3^{D286A} kinase-dead mutant. *C*, schematic of Vps34-Sgk3 coupled kinase assay. Phosphorylation of Crosstide was assayed by phosphorimaging. PI3P synthesis was measured by liquid scintillation. *D*, Vps34-Sgk3 coupled kinase assay. Crosstide phosphorylation was measured in the presence (*full blue line*) or absence (*dashed blue line*) of 50 nM Vps34. At the same time, PI3P synthesis was measured in the presence (*full green line*) or absence (*dashed green line*) of 50 nM Vps34. The binding of Sgk3 to the liposomes was determined by a liposome pelleting assay at the indicated time points following termination of the reaction with 2.5 mM EDTA (black curve). Error bars are the standard deviation of three independent experiments.

shown that PI(3,4,5)P_3 or PI(3,4)P_2 binding relieves pleckstrin homology (PH) domain-induced steric occlusion of the kinase domain catalytic cleft, leading to Akt activation (34, 35). To verify whether this is also the case for Sgk3, we performed hydrogen–deuterium exchange mass spectrometry (HDX-MS) on full-length Sgk3 and Sgk3 PX domain in the presence of vesicles containing 0 or 5 mol % PI3P. Binding of the isolated PX domain to PI3P vesicles led to dramatically lower exchange rates for peptides across the domain, including the PI3P-binding site, indicating that PI3P binding is captured by HDX-MS analysis (Fig. 3*A*). We next compared the HDX rates between full-length Sgk3^{WT} and the isolated PX domain to determine whether they interact with each other. We observed dramatic deprotection of the PX domain in the absence of the kinase domain of Sgk3 (Fig. 3*B*), indicating that the PX domain is sequestered in an intramolecular interaction in the full-length protein. Finally, we monitored HDX changes in full-length Sgk3 upon PI3P binding. Protection of the PX domain upon membrane binding was also observed, accompanied by deprotection in several areas of the kinase domain.

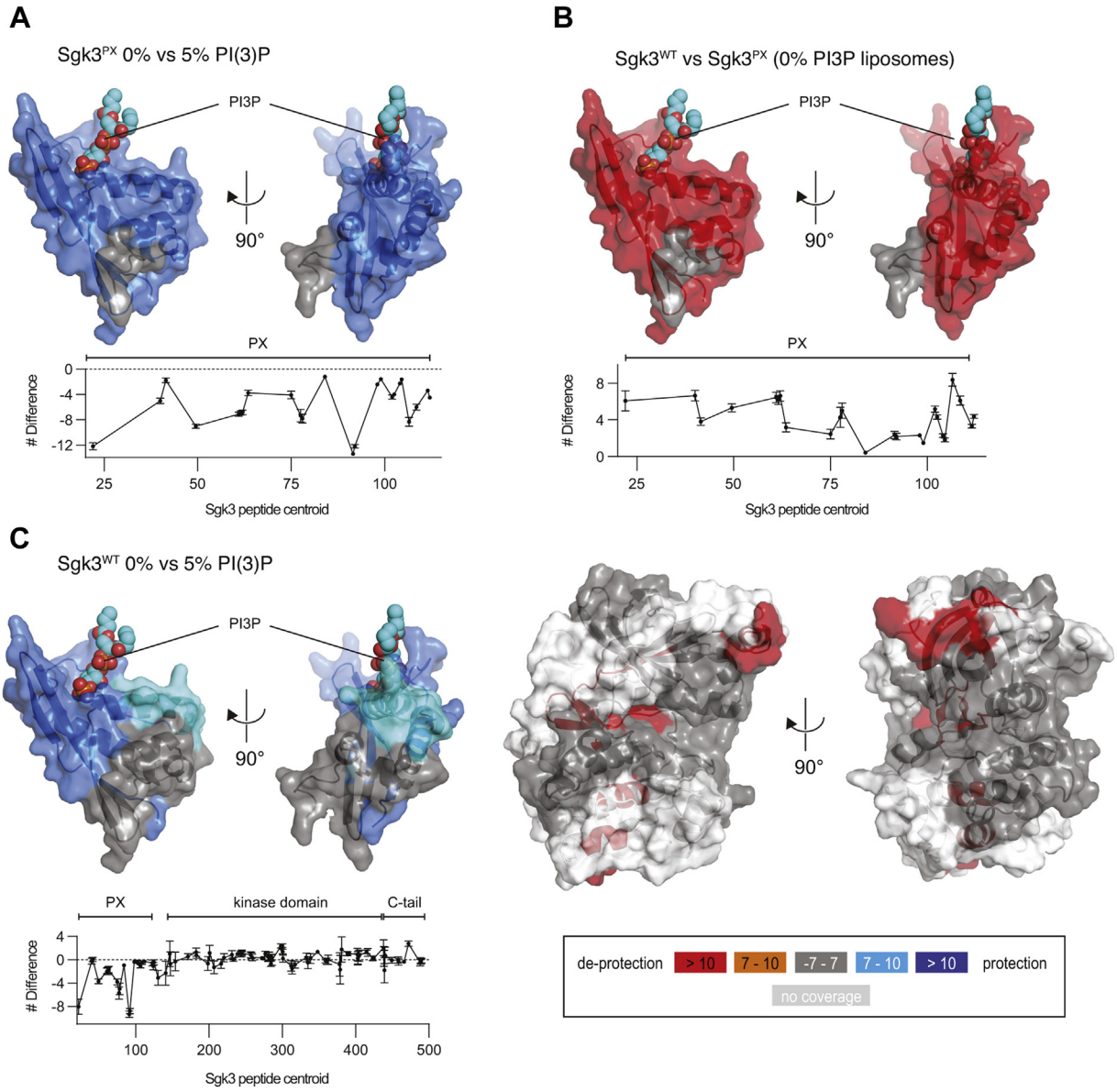

Figure 3. Sgk3 is autoinhibited by its PX domain. *A*, comparison of deuterium incorporation in Sgk3 PX domain with 0% *versus* 5% PI3P liposomes. Plot: difference in number of deuterons incorporated as a function of peptide centroid (defined as the amino acid number corresponding to the center of each peptide) over the PX domain. Negative numbers indicate protection (*blue*). Peptides showing significant deuterium exchange differences (>7%, >0.5 Da, and $p < 0.01$) were mapped on the structure of the human Sgk3 PX domain (PDB:6EDX). The binding site for PI3P is indicated by superimposing the structure of the PX domain of p40phox in complex with PI3P (PDB: 1H6H) and rendering the PI3P in spheres. *B*, comparison of deuterium incorporation in $Sgk3^{WT}$ *versus* Sgk3 PX domain in the presence of 0% PI3P liposomes (unbound). Plot: difference in number of deuterons incorporated as a function of peptide centroid over the PX domain. Positive numbers indicate domain exposure (*red*). *C*, comparison of deuterium incorporation in $Sgk3^{WT}$ unbound (0% PI3P) *versus* bound (5% PI3P) for the PX domain (*left*) and the kinase domain (*right*). A homology model of Sgk3 kinase domain (Rosetta) (75) was used to map the changes. Color coding expressing the magnitude of changes in deuterium incorporation is on bottom right. All measurements were done in triplicates, error bars are the standard deviations.

These sites form a contiguous network starting with β5, β7, and β8 strands in the N-lobe and propagating to the C-lobe *via* the αG and αI helices (Fig. 3*C*). Additional deprotection was observed in residues 468–476 localized in the C-terminal tail. It was not possible to delineate a clear surface of interaction between the PX and kinase domains from the changes in exchange rates in the kinase domain, but the data, taken together, provide unambiguous evidence for an intramolecular PX-kinase domain interaction and a large conformational change upon PI3P binding.

Autoinhibition of Sgk3 impairs binding to PI3P

Many AGC kinases that are activated by lipid second messengers exhibit a closed conformation of their autoinhibited state in which the binding site for the lipid headgroup is sequestered in an intramolecular interaction. To investigate whether the autoinhibited conformation of Sgk3 might also sequester the PI3P-binding site of its PX domain in intramolecular contacts, we compared the binding affinity for PI3P-containing liposomes of full-length Sgk3 and its isolated PX domain (Fig. S3*A*). To ensure identical conditions, we

incubated both proteins with PI3P liposomes in a single reaction, pelleted the liposomes, resolved the proteins in the supernatant and pellet fraction by SDS-PAGE, and quantified their abundance by Coomassie stain densitometry. To compensate for the lower staining sensitivity of the PX domain, we used an N-terminally FITC-labeled version of this construct (Fig. S3*B*) and quantified its fluorescence intensity in the gel before Coomassie staining (Fig. S3, *C* and *D*). We observed an approximately 5-fold higher affinity to PI3P of the isolated PX domain over the full-length protein (Fig. 4*A*), confirming that the PI3P-binding site is sequestered by the kinase domain in the autoinhibited state.

To substantiate this finding *in vivo*, we expressed mCherry-Sgk3^{WT} and eGFP-Sgk3^{PX} in HeLa cells and imaged their localization in serum-starved cells by confocal microscopy. While serum starvation of the cells overnight did not reduce PI3P levels sufficiently to dissociate Sgk3 from endosomes (Fig. 1*A*), it was clear that the isolated Sgk3 PX domain associates almost exclusively with endosomes (Fig. 4*B*), while full-length Sgk3 exhibits a predominantly cytosolic distribution (Fig. 4*C*). A representative cross section intensity trace for both channels reveals that the bulk of full-length Sgk3 is uniformly distributed in the cytoplasm of cells, while the PX domain is exclusively found on endosomes (Fig. 4, *D* and *E*). These findings confirm that the PI3P-binding pocket is sequestered in the autoinhibited conformation of Sgk3.

Discussion

Sgk3 is dependent on both PI3P and phosphorylation for its activity. We have shown here that Sgk3 exhibits negligible activity in the absence of activation loop phosphorylation and that PI3P significantly increases the basal activity of pre-phosphorylated Sgk3. Like other AGC kinases regulated by phospholipids, including Akt and PKC, the PI3P-binding pocket of the PX domain of Sgk3 is sequestered in an autoinhibitory, intramolecular conformation. This both necessitates PI3P for activity and simultaneously raises the threshold level of PI3P that must be reached in the cell in order to activate Sgk3. Like Sgk3, Akt1 is maintained in an autoinhibitory conformation by an intramolecular interaction that obscures its PIP_3-binding site, thereby impairing its binding to PIP_3 *in vitro* and *in vivo* (34). Similarly, the diacylglycerol (DAG)-binding site of the C1b domain of PKCβII is blocked by intramolecular contacts that impair its membrane translocation in response to phorbol ester treatment (40). More generally, the regulatory C1 domains of all PKC isozymes, as well as those of the PKD family, are engaged in autoinhibitory intramolecular interactions that impair their binding to membranes (41–43). Mechanistically, Sgk3 exhibits many of the features previously described for Akt, though given the structural divergence between the PX domain of Sgk3 and the PH domain of Akt, the atomistic details of autoinhibition are likely to be different. Sgk3 is the only Sgk to comprise a full PX domain, although Sgk1 has been shown to possess a short "PX-like" domain in its N-terminus that mediates lipid binding (44). Importantly, activation loop phosphorylation by PDK1 is insufficient to override the requirement for PI3P for full Sgk3 activity, a property also shared by Akt (35).

While not the major focus of this study, it is worth noting that turn motif phosphorylation of Sgk3 could not be observed in Sgk3 expressed either in insect or in human cells. This finding was unexpected, given the prominent role of turn motif phosphorylation in other AGC kinases. Phosphorylation of the turn motif helps to anchor the C-terminal tail of the kinase domain and increase the affinity of the phosphorylated hydrophobic motif to its cognate hydrophobic pocket in the N-lobe *via* local concentration, which leads to the overall

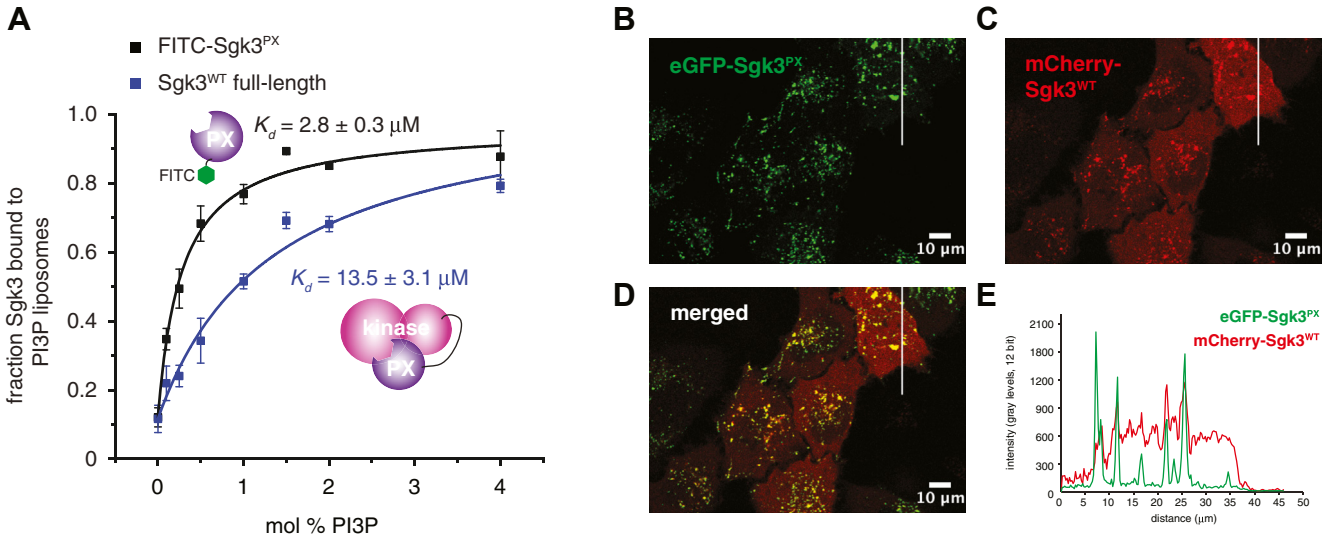

Figure 4. Autoinhibition of Sgk3 impairs binding to PI3P. *A*, binding of Sgk3^{WT} full-length (*blue squares*) and FITC-labeled Sgk3 PX domain (*black squares*) to 0–4 mol % PI3P liposomes was monitored in single reaction using fluorescence (FITX-PX) or Coomassie densitometry (full-length Sgk3) in 15% SDS-PAGE gels. Curves were fitted with a one binding site model. Error bars are the standard deviations of three independent experiments. *B–D*, distribution of eGFP-PX domain (*B*) or mCherry-Sgk3^{WT} (full-length) (*C*) in serum-starved HeLa cells. All images are representative of three independent transfections and multiple fields of view. *E*, quantification of fluorescence intensity of both constructs along the white line shown in images *B–D*.

stabilization of the kinase fold (33). While turn motif phosphorylation has been reported in all PKC isoforms, Akt, Sgk1, and PKN (45), whether it plays a role in Sgk3 regulation will require further investigation. Finally, it should also be noted that while hydrophobic motif phosphorylation has been reported to increase the catalytic activity of Sgk3 (17), which is entirely consistent with previous studies on the role of hydrophobic motif phosphorylation in Akt and PKC, our study does not address its contribution to Sgk3 activation.

Evidence suggests that PI3P binding by Sgk3 also promotes PDK1-dependent phosphorylation of its activation loop. This mechanism of activation loop exposure upon membrane binding is well established for Akt (46, 47). The requirement of PI3P for Sgk3 activity is therefore threefold: in the first place, it is required to target Sgk3 to membranes where it can encounter active PDK1; secondly, PI3P binding triggers a conformational change that renders it a substrate for PDK1; thirdly, and importantly, it is required to prevent autoinhibition of the kinase domain by the PX domain. Studies on Akt have also implicated ATP in stabilizing a phosphatase-resistant conformation of the kinase domain (48–50), a mechanism that we recently showed to be dependent on binding to membrane-embedded PIP_3 (35). While such a mechanism has not been explicitly shown for Sgk3, the homology between the kinase domains and the mechanisms by which Akt and Sgk3 are activated suggests that this is also likely to be the case for Sgk3 bound to PI3P-rich endosomes.

Our findings suggest that PI3P and phosphorylation are both required for Sgk3 activity, which makes Sgk3 a coincidence detector of both PI3P and PDK1. According to this model, PI3P-decorated endosomes lacking PDK1 would not serve as signaling hubs for Sgk3. In this respect, it is worth noting that PDK1 does not bind to, nor can it be activated by, PI3P. PDK1 binds with almost equal affinity to both $PI(3,4,5)P_3$ (1.6 nM) and $PI(3,4)P_2$ (5.2 nM) (51), which targets it to both the plasma membrane, which is abundant in PIP_3, and endomembranes, which are decorated with $PI(3,4)P_2$ and heavily implicated in Akt signaling (18, 34, 52, 53). PI3P is generally not observed at the plasma membrane. Presumably, PDK1 and Sgk3 cooperate to drive Sgk3 signaling on endosomes containing both $PI(3,4)P_2$ and PI3P (Fig. 5). Indeed, PDK1 has also been reported to associate with endosomes dependent on Sgk3 hydrophobic motif phosphorylation, where it inhibits ligand-induced degradation of the chemokine receptor CXCR4 (54). Sgk3 activity could therefore be restricted to a subpopulation of endosomes with a specific phosphoinositide composition. Interestingly, a recent large-scale analysis of human PX domains revealed the presence of a secondary lipid-binding site in the PX domain of Sgk3, which exhibits low-affinity $PI(3,4)P_2$ binding (30). The functional importance of the second lipid-binding site is still unclear, though one could easily imagine that it might serve to either fine-tune the lipid-binding specificity or increase binding affinity *via* an avidity effect (55).

A similar model for $PI(3,4)P_2$-driven Akt activity on endomembranes has recently been proposed to explain the transduction of growth factor signaling by Akt at subcellular locations distal to the plasma membrane. In this model, both

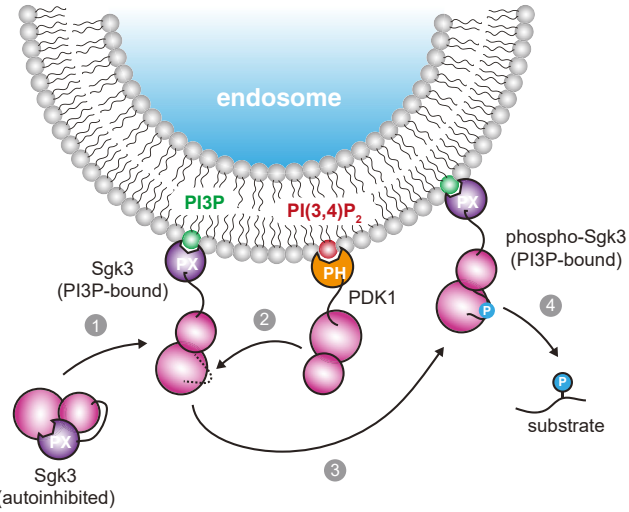

Figure 5. Model for the allosteric activation of Sgk3 by PI3P. Cytosolic Sgk3 is allosterically inhibited by its PX domain, which is relieved by PI3P binding (1). This is followed by phosphorylation of the Sgk3 activation loop by PDK1 as a consequence of its association with endosomal $PI(3,4)P_2$ (2). Phosphorylation activates Sgk3 (3), thereby permitting downstream substrate phosphorylation (4).

PDK1 and Akt are targeted to $PI(3,4)P_2$-containing endomembranes, where they cooperate to drive Akt signaling in the interior of the cell. Quantitative lipid imaging has revealed that endosomal pools of $PI(3,4)P_2$ are signaling hubs for Akt (18). Like Sgk3, Akt activity depends strictly on phosphorylation and the binding of its PH domain to either PIP_3 or $PI(3,4)P_2$, thereby confining its activity to membranes enriched in these signaling lipids (34, 35, 56).

Such a model of localized Sgk3 activity may provide an explanation for the reported overlap in Akt and Sgk3 substrate specificity (11, 15, 57, 58). Notwithstanding the similarity in their kinase domains, it is clear that their activity profiles would overlap in such a model, since the $PI(3,4)P_2$ that drives PDK1 and Akt activation must be present in membranes that support PI3P- and PDK1-mediated Sgk3 activation. Indeed, a recent phosphoproteomic study identified several Sgk3-specific substrates localized on endosomes (59). The reported role of Sgk3 in driving human cancers in the absence of Akt hyperactivation is then also reconcilable with this model and reinforces the potential value of Sgk3 as a therapeutic target either as a monotherapy or in combination with Akt inhibitors.

The chemical toolkit for Sgk3 inhibition is still limited due to similarities with other AGC kinases, such as Akt, and indeed with Sgk1 and Sgk2. However, inhibitor 14h has been reported to target all three Sgk isoforms without inhibiting Akt (9), and more recently, an Sgk3-specific PROTAC degrader has been described (60). Much effort has been aimed at developing allosteric inhibitors of Akt that specifically target the autoinhibited conformation of the kinase (61–63), although despite high oral bioavailability and specificity, none have yet made it to phase III clinical trials (64). Nevertheless, the identification of an autoinhibitory intramolecular interface in Sgk3, analogous but not homologous to Akt, presents opportunities for

the development of Sgk3-specific inhibitors that may have clinical value in the treatment of cancers in which Sgk3 signaling is observed to be upregulated. Such studies will undoubtedly benefit from the high-resolution structure determination of full-length, autoinhibited Sgk3.

Experimental procedures

Fluorescence microscopy

For localization studies of Sgk3 in live cells, HeLa cells were cotransfected with mCherry-Sgk3 (wt) and either eGFP-Sgk3^{PX} (residues 1–124) or eGFP-Sgk3^{R90A}. Cells were transfected using Turbofect transfection reagent according to the manufacturer's protocol. Cells were serum-starved overnight and changed into HBSS for live imaging. Images were acquired 24 h after transfection on a Zeiss LSM710 or LSM 700 confocal microscope equipped with a Zeiss 63× oil immersion objective (NA 1.4) and 488 and 561 nm lasers. Image processing and analysis were done using ImageJ 1.51j. All adjustments were applied uniformly across the entire image; no nonlinear adjustments were used.

Protein expression and purification

Sgk3 PX domain (residues 1–124) was cloned into pHisparallel bacterial expression vector and transformed into *E. coli* BL21 STAR electrocompetent cells. For large-scale expression, the cells were grown in LB medium containing 100 μg/ml ampicillin at 37 °C/180 RPM shaking, until OD_{600} reached 0.6. The temperature was lowered to 20 °C, expression was induced by the addition of 0.1 mM IPTG, and cells were grown overnight. Cells were harvested by centrifugation at 4000*g*/20 min, the pellet was flash-frozen in LN2 and stored at −80 °C for further use. Pellet corresponding to 1 l of culture was resuspended in 100 ml PX lysis buffer: 50 mM Tris pH 7.5, 150 mM NaCl, 20 mM imidazole, 1% (v/v) glycerol, 1 mM TCEP, 1 mM PMSF, 1 mM benzamidine hydrochloride, 2 mM $MgCl_2$, 1× protease inhibitor cocktail (made in-house: 100 μM bestatin, 14 μM E-64, 10 μM pepstatin A, and 1 μM phosphoramidon), 5 μl Denarase. The cell suspension was sonicated on ice, spun at 38,724*g*, 4 °C for 30 min. The soluble fraction was loaded on a HisTrap FF 5 ml column (Cytiva) equilibrated in NiA buffer: 50 mM Tris pH 7.5, 150 mM NaCl, 20 mM imidazole, 1% (v/v) glycerol, 1 mM TCEP. The column was washed with 20 column volumes (CVs) of NiA, ten CVs of high salt wash buffer (NiA +500 mM NaCl), an additional ten CVs of NiA, and the bound protein eluted with 0.02–1 M imidazole gradient over ten CVs. Fractions containing His-tagged PX domain were pooled and diluted with SA buffer (50 mM Hepes pH 8.0, 1% glycerol, 1 mM TCEP). The His tag was cleaved with TEV protease (made in-house) overnight at 4 °C. The cleaved protein was loaded on HiTrap SP HP 1 ml cation exchange column (Cytiva) equilibrated in SA buffer. The column was washed with ten CVs of SA and eluted with a 0–1 M NaCl gradient over 20 CVs. Fractions containing the PX domain were diluted with SA to adjust NaCl concentration to 150 mM and were either used for Sortase labeling (see below) or concentrated to 20 mg/ml, snap-frozen in LN2, and stored at −80 °C for further use.

Purified PX domain was specifically labeled on its N-terminal glycine with a FITC-LPETGG peptide (Genscript) in a Sortase-mediated reaction according to the protocol described in (65). Briefly, the PX domain was incubated with a 10-fold excess of FITC-LPETGG peptide in the presence of His-tagged Sortase A (prepared in-house) and 5 mM $CaCl_2$ at 4 °C overnight. Sortase was removed by NiNTA affinity chromatography and the labeled PX domain purified from free label by size-exclusion chromatography on a Superdex 75 10/300 column equilibrated in 20 mM Tris pH 8, 150 mM NaCl, 1% (v/v) glycerol, 20 mM imidazole, 1 mM TCEP. Fractions containing FITC-labeled PX domain were pooled, concentrated to 0.8 mg/ml, snap-frozen in LN2, and stored at −80 °C.

The human Sgk3 gene was codon optimized for expression in insect cells (Genscript) and fused to the C-terminus of His_{10}/StrepII-tagged eGFP (A206 K monomeric variant) to aid expression of soluble Sgk3. Both wild-type and kinase-dead (D286A) Sgk3 were coexpressed with PDK1 using a pFastBac Dual vector in baculovirus-infected Sf9 insect cells grown in ESF 921 medium (Expression Systems) at 27 °C. Bacmids were prepared from *Escherichia coli* DH10EMBacY cells containing a modified bacmid for titer determination of baculovirus using YFP expressed from a polyhedrin promoter in the baculoviral genome (66). Sf9 cells were transfected with bacmid using Fugene (Promega), and two rounds of viral amplification were performed in 2 ml adherent (1×10^6 cells/well) and 25 ml suspension (1×10^6 cells/ml) cultures to generate a V1 virus. For infection of Sf9 cells for recombinant protein expression, suspension cells (1L) were grown to a density of 2×10^6 cells/ml in Schott Duran 2L flasks before infection with 2 ml of V1 virus. Cells grew at 27 °C, shaking at 100 rpm until viability was approximately 80%. Cells were typically harvested 4–5 days postinfection. Wild-type and D286A constructs were purified under identical conditions. Briefly, the pellet of 0.5 l Sf9 cells was resuspended in 50 ml Sgk3 lysis buffer: 50 mM Hepes pH 7.4, 50 mM NaCl, 1% (v/v) glycerol, 1 mM TCEP, 1 mM PMSF, 1 mM benzamidine hydrochloride, 1 mM $MnCl_2$, 0.5 mM EDTA, 1× protease inhibitor cocktail, 0.1% CHAPS, 5 μl Denarase, 10 mM DTT, 1× protease inhibitor cocktail, 5 μl Denarase, 80 nM lambda phosphatase (made in-house). The lysate was passed through a Dounce homogenizer several times and spun at 38,724*g* (18,000 RPM), 4 °C for 30 min. The soluble fraction was loaded onto a StrepTrap HP 5 ml column (Cytiva) equilibrated in 50 mM Hepes pH 7.4, 50 mM NaCl, 1% (v/v) glycerol, 1 mM TCEP. The column was washed with ten CVs of binding buffer and the protein eluted with 2.5 mM *d*-desthiobiotin in binding buffer. Fractions containing EGFP-Sgk3 were pooled and dephosphorylated with lambda phosphatase in 50 mM Hepes pH 7.4, 150 mM NaCl, 1% (v/v) glycerol, 10 mM DTT, 1 mM $MnCl_2$, 0.5 mM EDTA, 0.5 μM lambda phosphatase (made in-house). Dephosphorylation was carried out for 30 min at room temperature and 4 °C overnight together with TEV cleavage of the His_{10}/StrepII tag. To separate His-tagged lambda phosphatase from Sgk3, the reaction mixture was loaded on HisTrap FF

1 ml column equilibrated in 20 mM Tris pH 7.4, 150 mM NaCl, 1% (v/v) glycerol, 1 mM TCEP. Dephosphorylated and cleaved Sgk3 was washed from the column with 20 mM imidazole, while lambda phosphatase remained bound. Sgk3 was then site-specifically *in vitro* re-phosphorylated by GST-PDK1 under the following conditions: 50 mM Tris pH 7.4, 150 mM NaCl, 1% (v/v) glycerol, 1 mM TCEP, 1 mM ATP, 2 mM $MgSO_4$, 1:10 PDK1:Sgk3. The reaction was carried out at 4 °C for 3 h, then stopped by addition of 10 mM EDTA. GST-PDK1 was separated by addition of glutathione-sepharose 4B beads (Cytiva) and incubation at 4 °C overnight with gentle rotation. Supernatant containing re-phosphorylated Sgk3 was concentrated in 30 kDa MWCO spin concentrator and injected onto a Superdex 200 Increase 10/300 GL column (Cytiva) equilibrated in 20 mM Tris pH 7.4, 150 mM NaCl, 1% (v/v) glycerol, 1 mM TCEP. Fractions containing Sgk3 were pooled, concentrated, snap-frozen in LN2, and stored at −80 °C for further use.

For the purification of Sgk3 from mammalian cells, an N-terminal GST fusion of $Sgk3^{WT}$ cloned into pLexm was expressed in transiently transfected HEK 293T cells as described previously (67). Purification was carried out under stringent phosphatase inhibition conditions to preserve any phosphorylation sites present. Cell pellets were lysed in buffer containing 50 mM Tris pH 7.4, 100 mM NaCl, 50 mM NaF, 2 mM benzamidine hydrochloride, 10 mM β-glycerophosphate, 2 mM sodium pyrophosphate, 2 mM sodium orthovanadate, 2 mM $MgCl_2$, 1 mM TCEP, benzonase (7.5 U/ml), 1× protease inhibitor cocktail. Lysate was pre-cleared with centrifugation at 38,724*g* (18,000 RPM), 4 °C for 30 min. Supernatant containing GST-$Sgk3^{WT}$ was bound to glutathione-sepharose 4B beads (Cytiva) for 2 h at 4 °C. Beads were washed 3× with the lysis buffer and finally resuspended in 50 mM Tris pH 7.4, 150 mM NaCl, 1 mM TCEP. Protein was cleaved from the beads with TEV protease overnight at 4 °C. Sgk3 was further purified by anion exchange chromatography before being subjected to GluC digest for MS/MS phosphomapping.

Recombinant baculovirus encoding Vps34 complex I (Atg6, protein A-tagged Atg14, Vps15, and Vps34) (68) was used to infect 3 L of Sf9 insect cell culture. Cells were harvested 4–5 days post-infection. Pellets were lysed in 300 ml of Vps34 lysis buffer: 50 mM Tris pH 8.8, 300 mM NaCl, 1 mM DTT, 0.5% CHAPS, 1 mM $MgCl_2$, 0.5 mM PMSF, 1× protease inhibitor cocktail, 15 µl Denarase. The lysate was passed several times through a Dounce homogenizer and spun at 38,724*g* (18,000 RPM), 4 °C for 30 min. The soluble fraction was bound to IgG-Sepharose beads (Cytiva) for 1 h at 4 °C with gentle rotation. Resin was collected in a gravity flow column and washed 3 × 50 ml wash buffer 1 (50 mM Tris pH 8, 300 mM NaCl, 1 mM DTT, 0.5% CHAPS, 0.5 mM PMSF), 2 × 50 ml wash buffer 2 (50 mM Tris pH 8, 300 mM NaCl, 1 mM DT, 2% (v/v) glycerol, 0.25% CHAPS). Finally, beads were resuspended in wash buffer 2 and bound protein complex cleaved with TEV at 4 °C overnight. The supernatant containing the full Vps34 complex was concentrated and injected onto a Superdex 200 Increase 10/300 GL column equilibrated in 50 mM Tris pH 8, 150 mM NaCl, 1 mM TCEP, 2% (v/v) glycerol. Fractions containing the complete complex of Atg6, Atg14, Vps15, and Vps34 were pooled, concentrated to 0.9 mg/ml, snap-frozen in LN2, and stored at −80 °C for further use.

Intact mass spectrometry

Intact protein samples were diluted in H_2O and up to 100 ng protein was loaded on an XBridge Protein BEH C4 column (2.5 µm particle size, dimensions 2.1 mm × 150 mm; Waters) using a Dionex Ultimate 3000 HPLC system (Thermo Fisher Scientific) with a working temperature of 50 °C, 0.1% formic acid (FA) as solvent A, 80% acetonitrile, 0.08% FA as solvent B. Proteins were separated with a 6 min step gradient from 10 to 80% solvent B at a flow rate of 300 µl/min and analyzed on a Synapt G2-Si coupled *via* a ZSpray ESI source (Waters). Data were recorded with MassLynx V 4.1 (Waters) and analyzed using the MaxEnt 1 process to reconstruct the uncharged average protein mass.

Tandem mass spectrometry

The reduced protein was denatured in 4 M urea, 50 mM ammonium bicarbonate (ABC) and alkylated with 20 mM iodoacetamide for 30 min at room temperature in the dark. The sample was diluted with 50 mM ABC down to 0.5 M urea and then digested overnight using sequencing-grade endoproteinase GluC (Roche) at 25 °C. The digestion was stopped by adding trifluoroacetic acid to a final concentration of 1%, and the peptides were desalted using custom-made C18 stagetips (69). The peptides were separated on an Ultimate 3000 RSLC nanoflow chromatography system (Thermo Fisher Scientific), using a precolumn for sample loading (PepMapAcclaim C18, 2 cm × 0.1 mm, 5 µm) and a C18 analytical column (PepMapAcclaim C18, 50 cm × 0.75 mm, 2 µm, both Dionex-Thermo Fisher Scientific), applying a linear gradient from 2 to 35% solvent B (80% acetonitrile, 0.08% FA acid; solvent A: 0.1% FA) at a flow rate of 230 nl/min over 60 min. Eluting peptides were analyzed on a Q Exactive HF or HF-X Orbitrap mass spectrometer equipped with a Proxeon nanospray source (Thermo Fisher Scientific), operated in data-dependent mode. Survey scans were obtained in a scan range of 375–1500 m/z, at a resolution of 60,000 at 200 m/z and an AGC target value of 3E6. The eight most intense ions were selected with an isolation width of 1.6 Da, fragmented in the HCD cell at 28% collision energy and the spectra recorded at a target value of 1E5 and a resolution of 30,000. Peptides with a charge of +1 were excluded from fragmentation, the peptide match and exclude isotope features were enabled and selected precursors were dynamically excluded from repeated sampling. Raw data were processed using the MaxQuant software package (version 1.6.0.16, http://www.maxquant.org/) (70) and searched against a custom database containing the sequences of the Sgk3 constructs in the protein background of the expression system plus the sequences of common contaminants. The protein background sequences were extracted from www.uniprot.org: *Spodoptera* spp. protein sequences plus the *Bombyx mori* reference proteome (2014.01; 16,269 entries) or the human proteome (2019.01_UP000005640_9606_Homo_

sapiens_all.fasta; 95,977 entries). The search was performed with C-terminal cleavage to glutamate and aspartate allowing four missed cleavages. Carbamidomethylation of cysteine residues was set as fixed, oxidation of methionine, protein N-terminal acetylation, and phosphorylation of serine, threonine, and tyrosine as variable modifications—all other parameters were set to default. The precursor tolerance was set to 4.5 ppm, the fragment mass tolerance to 20 ppm. Results were filtered at a false discovery rate of 10% at the peptide and protein level. Spectra of phosphorylated Sgk3 peptides were validated manually. All proteomics data have been deposited in the PRIDE repository (71) with the identifier PXD026281.

Size-exclusion chromatography with multiangle light scattering (SEC-MALS)

Sgk3 (80 μl) at 0.9 mg/ml was injected onto Superdex 200 Increase 10/300 GL column (Cytiva) equilibrated in 20 mM Tris pH 8, 150 mM NaCl, 1% (v/v) glycerol, 1 mM TCEP. Separation was carried out using HPLC Agilent Technologies 1260 infinity with a flow rate of 0.5 ml/min operated at room temperature. Online light scattering of 690 nm laser was recorded on a miniDawn Treos detector (Wyatt Technology Corp.). Shodex RI-101 (Shodex) refractive index detector was used to measure protein concentration online. Data was analyzed using the ASTRA software (Wyatt Technology Corp.).

Dynamic light scattering (DLS)

Autocorrelation curves of freshly thawed and centrifuged 7.5 μM Sgk3 in buffer containing 20 mM Hepes pH 7.4, 150 mM NaCl, 1% (v/v) glycerol, 1 mM TCEP, 1 mM ATP, 2 mM $MgCl_2$, 100 μM Crosstide were recorded at 0 and 60 min of incubation at room temperature. Measurements were performed on a DynaPro NanoStar instrument (Wyatt Technology Corp.). Each measurement is an average of ten acquisitions of 10 s each.

Sucrose-loaded vesicles (SLVs)

Cholesterol, DOPC, DOPE, DOPS, and liver PI were dissolved in chloroform, PI3P di C16 was dissolved in chloroform:methanol:water 1:2:0.8, $PI(4,5)P_2$ was dissolved in chloroform:methanol:water 20:13:3. For liposomes with synthetic PI3P the lipids were mixed in the following molar ratio: 20% cholesterol, 30% DOPC, 15% DOPS, 35% DOPE. For liposomes containing PI3P, DOPC was substituted with 0–4% PI3P. Liver PI liposomes contained 10% PI at the expense of DOPC. Lipid mixtures in borosilicate glass tubes were evaporated with nitrogen to form a thin film and then rehydrated by vortexing for 1 min with sucrose buffer (20 mM Hepes pH 7.4, 300 mM sucrose). Resuspended lipids were subjected to four cycles of freezing in LN2 and thawing in a sonicator bath. One volume of gel filtration buffer was added and liposomes were pelleted in Beckman Coulter Optima MAX-XP Ultracentrifuge in TLA 100 rotor operated at 50,000 rpm/20 °C for 30 min. The supernatant was discarded, liposome pellets were resuspended in gel filtration buffer to a final lipid concentration of 1 mM, and stored for a maximum of 2 days at 4 °C before use.

Radiometric kinase assays

Sgk3 kinase activity was monitored as the incorporation of radioactive phosphate from γ^{32}P-ATP (Hartmann Analytic) into Crosstide (GRPRTSSFAEG), a validated Sgk3 substrate peptide. Sgk3 was mixed with PI3P-containing liposomes and incubated for 30 min at RT. In total, 5 μl of liposomes-Sgk3 mixture was added to 5 μl of substrate master mix to obtain following conditions: 20 mM Tris pH 8, 150 mM NaCl, 1% (v/v) glycerol, 1 mM TCEP, 50 nM Sgk3, 100 μM Crosstide, 1 mM ATP (spiked 1:10 with γ^{32}P-ATP), 2 mM $MgCl_2$. The reaction was left to proceed for 15 min at room temperature and stopped by addition of 2 μl of 0.5 M EDTA. In total, 10 μl of the reaction was then spotted onto a nitrocellulose membrane (0.2 μm pore size), washed 5 × 3 min with 75 mM H_3PO_4, and the washed membrane was inserted into a 20 ml polyethylene scintillation vial containing 5 ml deionized H_2O. Cerenkov radiation was measured in a Tri-Carb 4910 TR liquid scintillator (PerkinElmer). Datapoints were fitted with Michaelis–Menten equation modified with a constant to reflect the basal enzymatic activity in 0% PI3P condition:

$$V = \frac{V_{max}[PI3P]}{k_1 + [PI3P]} + const$$

Liposome pelleting assay

$Sgk3^{PX}$ or 1 μM $Sgk3^{WT}$ was mixed 1:1 with liposomes, incubated at 20 °C for 30 min, and spun at 9800*g* for 30 min at 20 °C. Supernatant was collected and the liposome pellet resuspended in gel filtration buffer. Equal volumes of supernatant and pellet fractions were separated by SDS-PAGE and quantified by Coomassie densitometry. In the comparative binding assay with full-length Sgk3 and $Sgk3^{PX}$ in the same reaction, FITC-labeled PX domain was quantified by fluorescence at 448 nm. Binding curves were fitted with a one-site binding model.

Vps34-Sgk3-coupled kinase assay

To monitor PI3P production by Vps34 and Crosstide phosphorylation by Sgk3 in a single reaction, the components were mixed at following concentrations: 50 nM Vps34 complex, 50 nM Sgk3, 500 μM Biotin-Crosstide, 0.5 mM ATP (spiked 1:10 with γ^{32}P-ATP), 0.5 mM $MgCl_2$, 2 mM $MnCl_2$, 1 mM EGTA, 10% liver PI liposomes. The reaction was carried out at 25 °C and gentle shaking; 15 μl samples were mixed with 5 μl 4× quench buffer (20 mM Tris pH 7.4, 150 mM NaCl, 10 mM EDTA, 10 mM EGTA, 1% (v/v) glycerol, 1 mM TCEP) at indicated time points. The quenched reactions were spun for 5 min at 20,800*g*/20 °C. The supernatant was mixed 1:1 with NeutrAvidin (Thermo Scientific) at 2 mg/ml in water to sequester the biotinylated Crosstide and 5 μl was spotted onto 0.45 μm nitrocellulose membrane. The membrane was washed 5 × 3 min with TBS (20 mM Tris pH 7.6, 137 mM

NaCl), briefly dried, exposed in storage phosphor screen overnight, and imaged with an Amersham Typhoon phosphorimager. The intensity of the spots was quantified in ImageJ. The pellets containing liposomes with $PI3^{32}P$ were washed four times with wash buffer (20 mM Tris pH 7.4, 150 mM NaCl, 2.5 mM EDTA, 2.5 mM EGTA, 1% (v/v) glycerol, 1 mM TCEP), transferred into PCR tube, and inserted into 20 ml polyethylene scintillation vials containing 5 ml MilliQ water. PI3P synthesis was measured by liquid scintillation.

HDX-MS

Lipid vesicle preparation

Lipid films containing 20% cholesterol, 25% DOPC, 15% DOPS, 35% DOPE, and 5% PI3P were dried and stored under argon for shipping. The dried films were resuspended to 5 mM in gel filtration buffer (20 mM Tris pH 7.4, 150 mM NaCl, 1% (v/v) glycerol, 1 mM TCEP) by vortexing. The resuspended lipid vesicle solutions were sonicated for 10 min, subjected to ten freeze–thaw cycles, and sonicated again for 5 min. The vesicles were then snap-frozen in liquid nitrogen and stored at −80 °C

HDX-MS sample preparation

HDX reactions were conducted in a final reaction volume of 25 μl with a final Sgk3 concentration of 13 μM (for both FL and PX Sgk3). Prior to the addition of deuterated solvent, 1.5 μl of FL or PX Sgk3 was allowed to incubate with either 2 μl of 5 mM 0% PI3P vesicles or 2 μl 5 mM 5% PI3P vesciles. After the 2 min incubation period, 21.5 μl D_2O buffer (20 mM pH 7 HEPES, 100 mM NaCl, 0.5 mM TCEP, 94% D_2O) was added with a final $\%D_2O$ of 81.5% (v/v). The reaction was allowed to proceed for 3 s, 30 s, 300 s, or 3000 s at 18 °C before being quenched with ice-cold acidic quench buffer. All conditions and time points were created and run in triplicate. Samples were flash-frozen in liquid nitrogen and stored at −80 °C until injection onto the ultraperformance liquid chromatography system for proteolytic cleavage, peptide separation, and injection onto a QTOF for mass analysis.

Protein digestion and MS/MS data collection

Protein samples were rapidly thawed and injected onto an integrated fluidics system containing an HDx-3 PAL liquid handling robot and climate-controlled chromatography system (LEAP Technologies), a Dionex Ultimate 3000 UHPLC system, as well as an Impact HD QTOF Mass spectrometer (Bruker). The protein was run over either one immobilized pepsin column at 10 °C (Trajan; ProDx protease column, 2.1 mm × 30 mm PDX.PP01-F32) at 200 ml/min for 3 min. The resulting peptides were collected and desalted on a C18 trap column (Acquity UPLC BEH C18 1.7 mm column (2.1 × 5 mm); Waters 186003975). The trap was subsequently eluted in line with a C18 reverse-phase separation column (Acquity 1.7 mm particle, 100 × 1 mm^2 C18 UPLC column, Waters 186002352), using a gradient of 5–36% B (Buffer A 0.1% formic acid; Buffer B 100% acetonitrile) over 16 min. Full details of the LC system are described in (72). Mass spectrometry experiments acquired over a mass range from 150 to 2200 m/z using an electrospray ionization source operated at a temperature of 200 °C and a spray voltage of 4.5 kV.

Peptide identification

Peptides were identified from the nondeuterated samples of FL and PX Sgk3 using data-dependent acquisition following tandem MS/MS experiments (0.5 s precursor scan from 150 to 2000 m/z; 12 0.25 s fragment scans from 150 to 2000 m/z). MS/MS data sets were analyzed using PEAKS7 (PEAKS), and peptide identification was carried out by using a false-discovery-based approach, with a threshold set to 1% using a database of composed of Sgk3, porcine pepsin, and known contaminants found in Sf9 cells (8 total protein sequences) (73). The search parameters were set with a precursor tolerance of 20 ppm, fragment mass error 0.02 Da, charge states from 1 to 8, leading to a selection criterion of peptides that had a −10logP score of 21.4.

Mass analysis of peptide centroids and measurement of deuterium incorporation

HD-Examiner Software (Sierra Analytics) was used to automatically calculate the level of deuterium incorporation into each peptide. All peptides were manually inspected for correct charge state, correct retention time, appropriate selection of isotopic distribution, etc. Deuteration levels were calculated using the centroid of the experimental isotope clusters. Results are presented as relative levels of deuterium incorporation, and the only control for back exchange was the level of deuterium present in the buffer (81.5%). Differences in exchange in a peptide were considered significant if they met all three of the following criteria: ≥7% change in exchange, ≥0.5 Da difference in exchange, and a p value <0.01 using a two-tailed Student's t test. All compared samples were set within the same experiment. To allow for visualization of differences across all peptides, we utilized number of deuteron difference (#D) plots. These plots show the total difference in deuterium incorporation over the entire H/D exchange time course, with each point indicating a single peptide. The mass spectrometry proteomics data have been deposited to the ProteomeXchange Consortium *via* the PRIDE partner repository (71) with the data set identifier PXD025327. The data analysis statistics for all HDX-MS experiments are in Table S1 according to the guidelines of Masson *et al.* (74).

Data availability

Mass spectrometry data associated with this manuscript have been deposited in the PRIDE repository with the identifiers PXD026281 (Mapping of phosphorylation sites on Sgk3

by LC-MS/MS) and PXD025327 (*In vitro* reconstitution of Sgk3 activation by phosphatidylinositol-3-phosphate).

Supporting information—This article contains supporting information.

Acknowledgments—Intact mass analyses and phosphorylation mapping experiments were performed by Dorothea Anrather and Thomas Gossenreiter from the Mass Spectrometry Facility at the Max Perutz Labs using instruments of the Vienna BioCenter Core Facilities (VBCF). We thank Justyna Sawa-Makarska and Sascha Martens (Max Perutz Labs) for their generous gift of baculovirus for the expression of the Vps34 complex.

Author contributions—T. A. L. conceptualization; D. P., K. D. F., and T. A. L. formal analysis; J. E. B. and T. A. L. funding acquisition; D. P., L. T., and K. D. F. investigation; D. P. and J. E. B. methodology; T. A. L. project administration; T. A. L. resources; T. A. L. supervision; T. A. L. visualization; D. P. and T. A. L. writing-original draft; D. P., L. T., J. E. B., and T. A. L. writing-review and editing.

Funding and additional information—This work was supported by the Austrian Science Fund (FWF) grants P28135, P30584, P33066, and W1261 to T. A. L. L. T. was supported by a Hertha Firnberg Postdoctoral Fellowship from the Austrian Science Fund (FWF T915). J. E. B. was supported by a Michael Smith Foundation for Health Research (MSFHR) Scholar award (17686) and an operating grant from the Cancer Research Society (CRS-24368).

Conflict of interests—The authors declare that they have no conflicts of interest with the contents of this article.

Abbreviations—The abbreviations used are: EEA1, early endosome antigen 1; GSK3β, glycogen synthase kinase-3 beta; HDX-MS, hydrogen–deuterium exchange mass spectrometry; INPP4, inositol polyphosphate-4-phosphatase; mTORC2, mammalian target of rapamycin complex 2; PDK1, 3-phosphoinositide-dependent protein kinase 1; PI(3,4)P_2, phosphatidylinositol 3,4,-bisphosphate; PI(3,4,5)P_3, phosphatidylinositol 3,4,5-trisphosphate; PI3K, phosphoinositide 3-kinase; PI3P, phosphatidylinositol 3-phosphate; PKC, protein kinase C; Sgk3, serum/glucocorticoid-regulated kinase 3; SHIP2, SH2-containing inositol 5′ phosphatase; Vps34, vacuolar protein sorting 34.

References

1. Martini, M., De Santis, M. C., Braccini, L., Gulluni, F., and Hirsch, E. (2014) PI3K/AKT signaling pathway and cancer: An updated review. *Ann. Med.* **46**, 372–383
2. Fruman, D. A., and Rommel, C. (2014) PI3K and cancer: Lessons, challenges and opportunities. *Nat. Rev. Drug Discov.* **13**, 140–156
3. Fruman, D. A., Chiu, H., Hopkins, B. D., Bagrodia, S., Cantley, L. C., and Abraham, R. T. (2017) The PI3K pathway in human disease. *Cell* **170**, 605–635
4. Marone, R., Cmiljanovic, V., Giese, B., and Wymann, M. P. (2008) Targeting phosphoinositide 3-kinase-Moving towards therapy. *Biochim. Biophys. Acta* **1784**, 159–185
5. Manning, G. (2002) The protein kinase complement of the human genome. *Science* **298**, 1912–1934
6. Endicott, J. A., Noble, M. E. M., and Johnson, L. N. (2012) The structural basis for control of eukaryotic protein kinases. *Annu. Rev. Biochem.* **81**, 587–613
7. Leonard, T. A., and Hurley, J. H. (2011) Regulation of protein kinases by lipids. *Curr. Opin. Struct. Biol.* **21**, 785–791
8. Liu, D., Yang, X., and Songyang, Z. (2000) Identification of CISK, a new member of the SGK kinase family that promotes IL-3-dependent survival. *Curr. Biol.* **10**, 1233–1236
9. Bago, R., Sommer, E., Castel, P., Crafter, C., Bailey, F. P., Shpiro, N., Baselga, J., Cross, D., Eyers, P. A., and Alessi, D. R. (2016) The hVps34-SGK3 pathway alleviates sustained PI3K/Akt inhibition by stimulating mTORC1 and tumour growth. *EMBO J.* **35**, 1902–1922
10. Kobayashi, T., and Cohen, P. (1999) Activation of serum- and glucocorticoid-regulated protein kinase by agonists that activate phosphatidylinositide 3-kinase is mediated by 3-phosphoinositide-dependent protein kinase-1 (PDK1) and PDK2. *Biochem. J.* **339**, 319–328
11. Kobayashi, T., Deak, M., Morrice, N., and Cohen, P. (1999) Characterization of the structure and regulation of two novel isoforms of serum- and glucocorticoid-induced protein kinase. *Biochem. J.* **344**, 189–197
12. Ikenoue, T., Inoki, K., Yang, Q., Zhou, X., and Guan, K.-L. (2008) Essential function of TORC2 in PKC and Akt turn motif phosphorylation, maturation and signalling. *EMBO J.* **27**, 1919–1931
13. Facchinetti, V., Ouyang, W., Wei, H., Soto, N., Lazorchak, A., Gould, C., Lowry, C., Newton, A. C., Mao, Y., Miao, R. Q., Sessa, W. C., Qin, J., Zhang, P., Su, B., and Jacinto, E. (2008) The mammalian target of rapamycin complex 2 controls folding and stability of Akt and protein kinase C. *EMBO J.* **27**, 1932–1943
14. Virbasius, J. V., Song, X., Pomerleau, D. P., Zhan, Y., Zhou, G. W., and Czech, M. P. (2001) Activation of the Akt-related cytokine-independent survival kinase requires interaction of its phox domain with endosomal phosphatidylinositol 3-phosphate. *Proc. Natl. Acad. Sci. U. S. A.* **98**, 12908–12913
15. Tessier, M., and Woodgett, J. R. (2006) Role of the Phox homology domain and phosphorylation in activation of serum and glucocorticoid-regulated kinase-3. *J. Biol. Chem.* **281**, 23978–23989
16. Xing, Y., Liu, D., Zhang, R., Joachimiak, A., Songyang, Z., and Xu, W. (2004) Structural basis of membrane targeting by the phox homology domain of cytokine-independent survival kinase (CISK-PX). *J. Biol. Chem.* **279**, 30662–30669
17. Bago, R., Malik, N., Munson, M. J., Prescott, A. R., Davies, P., Sommer, E., Shpiro, N., Ward, R., Cross, D., Ganley, I. G., and Alessi, D. R. (2014) Characterization of VPS34-IN1, a selective inhibitor of Vps34, reveals that the phosphatidylinositol 3-phosphate-binding SGK3 protein kinase is a downstream target of class III phosphoinositide 3-kinase. *Biochem. J.* **463**, 413–427
18. Liu, S.-L. L., Wang, Z.-G. G., Hu, Y., Xin, Y., Singaram, I., Gorai, S., Zhou, X., Shim, Y., Min, J.-H. H., Gong, L.-W. W., Hay, N., Zhang, J., and Cho, W. (2018) Quantitative lipid imaging reveals a new signaling function of phosphatidylinositol-3,4-bisphophate: Isoform- and site-specific activation of Akt. *Mol. Cell.* **71**, 1092–1104.e5
19. Goulden, B. D., Pacheco, J., Dull, A., Zewe, J. P., Deiters, A., and Hammond, G. R. V. (2018) A high-avidity biosensor reveals plasma membrane PI(3,4)P2 is predominantly a class I PI3K signaling product. *J. Cell Biol.* **218**, 1066–1079
20. Ivetac, I., Munday, A. D., Kisseleva, M. V., Zhang, X.-M., Luff, S., Tiganis, T., Whisstock, J. C., Rowe, T., Majerus, P. W., and Mitchell, C. A. (2005) The type Ialpha inositol polyphosphate 4-phosphatase generates and terminates phosphoinositide 3-kinase signals on endosomes and the plasma membrane. *Mol. Biol. Cell.* **16**, 2218–2233
21. Backer, J. M. (2008) The regulation and function of class III PI3Ks: Novel roles for Vps34. *Biochem. J.* **410**, 1–17
22. Malik, N., Macartney, T., Hornberger, A., Anderson, K. E., Tovell, H., Prescott, A. R., and Alessi, D. R. (2018) Mechanism of activation of SGK3 by growth factors via the Class 1 and Class 3 PI3Ks. *Biochem. J.* **475**, 117–135
23. Gewinner, C., Wang, Z. C., Richardson, A., Teruya-Feldstein, J., Etemadmoghadam, D., Bowtell, D., Barretina, J., Lin, W. M., Rameh, L., Salmena, L., Pandolfi, P. P., and Cantley, L. C. (2009) Evidence that inositol polyphosphate 4-phosphatase type II is a tumor suppressor that inhibits PI3K signaling. *Cancer Cell* **16**, 115–125
24. Webster, M. K., Goya, L., Ge, Y., Maiyar, A. C., and Firestone, G. L. (1993) Characterization of sgk, a novel member of the serine/threonine

protein kinase gene family which is transcriptionally induced by glucocorticoids and serum. *Mol. Cell. Biol.* **13**, 2031–2040
25. Lang, F., Bohmer, C., Palmada, M., Seebohm, G., Strutz-Seebohm, N., and Vallon, V. (2006) (Patho)physiological significance of the serum- and glucocorticoid-inducible kinase isoforms. *Physiol. Rev.* **86**, 1151–1178
26. Gasser, J. A., Inuzuka, H., Lau, A. W., Wei, W., Beroukhim, R., and Toker, A. (2014) SGK3 mediates INPP4B-dependent PI3K signaling in breast cancer. *Mol. Cell.* **56**, 595–607
27. Vasudevan, K. M., Barbie, D. A., Davies, M. A., Rabinovsky, R., McNear, C. J., Kim, J. J., Hennessy, B. T., Tseng, H., Pochanard, P., Kim, S. Y., Dunn, I. F., Schinzel, A. C., Sandy, P., Hoersch, S., Sheng, Q., *et al.* (2009) AKT-independent signaling downstream of oncogenic PIK3CA mutations in human cancer. *Cancer Cell* **16**, 21–32
28. Wang, Y., Zhou, D., Phung, S., Warden, C., Rashid, R., Chan, N., and Chen, S. (2017) SGK3 sustains ERα signaling and drives acquired aromatase inhibitor resistance through maintaining endoplasmic reticulum homeostasis. *Proc. Natl. Acad. Sci. U. S. A.* **114**, E1500–E1508
29. Xu, J., Liu, D., Gill, G., and Songyang, Z. (2001) Regulation of cytokine-independent survival kinase (CISK) by the phox homology domain and phosphoinositides. *J. Cell Biol.* **154**, 699–705
30. Chandra, M., Chin, Y. K. Y., Mas, C., Feathers, J. R., Paul, B., Datta, S., Chen, K. E., Jia, X., Yang, Z., Norwood, S. J., Mohanty, B., Bugarcic, A., Teasdale, R. D., Henne, W. M., Mobli, M., *et al.* (2019) Classification of the human phox homology (PX) domains based on their phosphoinositide binding specificities. *Nat. Commun.* **10**, 1528
31. Chen, W., Chen, Y., Xu, B. E., Juang, Y. C., Stippec, S., Zhao, Y., and Cobb, M. H. (2009) Regulation of a third conserved phosphorylation site in SGK1. *J. Biol. Chem.* **284**, 3453–3460
32. Oh, W. J., Wu, C., Kim, S. J., Facchinetti, V., Julien, L.-A., Finlan, M., Roux, P. P., Su, B., and Jacinto, E. (2010) mTORC2 can associate with ribosomes to promote cotranslational phosphorylation and stability of nascent Akt polypeptide. *EMBO J.* **29**, 3939–3951
33. Hauge, C., Antal, T. L., Hirschberg, D., Doehn, U., Thorup, K., Idrissova, L., Hansen, K., Jensen, O. N., Jørgensen, T. J., Biondi, R. M., and Frödin, M. (2007) Mechanism for activation of the growth factor-activated AGC kinases by turn motif phosphorylation. *EMBO J.* **26**, 2251–2261
34. Ebner, M., Lučić, I., Leonard, T. A., and Yudushkin, I. (2017) PI(3,4,5)P3 engagement restricts Akt activity to cellular membranes. *Mol. Cell.* **65**, 416–431.e6
35. Lučić, I., Rathinaswamy, M. K., Truebestein, L., Hamelin, D. J., Burke, J. E., and Leonard, T. A. (2018) Conformational sampling of membranes by Akt controls its activation and inactivation. *Proc. Natl. Acad. Sci. U. S. A.* **115**, E3940–E3949
36. Dai, F., Yu, L., He, H., Chen, Y., Yu, J., Yang, Y., Xu, Y. F., Ling, W., and Zhao, S. (2002) Human serum and glucocorticoid-inducible kinase-like kinase (SGKL) phosphorylates glycogen syntheses kinase 3 beta (GSK-3β) at serine-9 through direct interaction. *Biochem. Biophys. Res. Commun.* **293**, 1191–1196
37. Hastie, C. J., McLauchlan, H. J., and Cohen, P. (2006) Assay of protein kinases using radiolabeled ATP: A protocol. *Nat. Protoc.* **1**, 968–971
38. Hurley, J. H., and Young, L. N. (2017) Mechanisms of autophagy initiation. *Annu. Rev. Biochem.* **86**, 225–244
39. Backer, J. M. (2016) The intricate regulation and complex functions of the Class III phosphoinositide 3-kinase Vps34. *Biochem. J.* **473**, 2251–2271
40. Leonard, T. A., Róycki, B., Saidi, L. F., Hummer, G., and Hurley, J. H. (2011) Crystal structure and allosteric activation of protein kinase C βiI. *Cell* **144**, 55–66
41. Oancea, E., and Meyer, T. (1998) Protein kinase C as a molecular machine for decoding calcium and diacylglycerol signals. *Cell* **95**, 307–318
42. Lučić, I., Truebestein, L., and Leonard, T. A. (2016) Novel features of DAG-activated PKC isozymes reveal a conserved 3-D architecture. *J. Mol. Biol.* **428**, 121–141
43. Elsner, D. J., Siess, K. M., Gossenreiter, T., Hartl, M., and Leonard, T. A. (2019) A ubiquitin-like domain controls protein kinase D dimerization and activation by trans-autophosphorylation. *J. Biol. Chem.* **294**, 14422–14441
44. Pao, A. C., McCormick, J. A., Li, H., Siu, J., Govaerts, C., Bhalla, V., Soundararajan, R., and Pearce, D. (2007) NH 2 terminus of serum and glucocorticoid-regulated kinase 1 binds to phosphoinositides and is essential for isoform-specific physiological functions. *Am. J. Physiol. Physiol.* **292**, F1741–F1750
45. Hornbeck, P. V., Chabra, I., Kornhauser, J. M., Skrzypek, E., and Zhang, B. (2004) PhosphoSite: A bioinformatics resource dedicated to physiological protein phosphorylation. *Proteomics* **4**, 1551–1561
46. Alessi, D. R., Deak, M., Casamayor, A., Caudwell, F. B., Morrice, N., Norman, D. G., Gaffney, P., Reese, C. B., MacDougall, C. N., Harbison, D., Ashworth, A., and Bownes, M. (1997) 3-Phosphoinositide-dependent protein kinase-1 (PDK1): Structural and functional homology with the Drosophila DSTPK61 kinase. *Curr. Biol.* **7**, 776–789
47. Stokoe, D., Stephens, L. R., Copeland, T., Gaffney, P. R., Reese, C. B., Painter, G. F., Holmes, A. B., McCormick, F., and Hawkins, P. T. (1997) Dual role of phosphatidylinositol-3,4,5-trisphosphate in the activation of protein kinase B. *Science* **277**, 567–570
48. Lu, S., Deng, R., Jiang, H., Song, H., Li, S., Shen, Q., Huang, W., Nussinov, R., Yu, J., and Zhang, J. (2015) The mechanism of ATP-dependent allosteric protection of Akt kinase phosphorylation. *Structure* **23**, 1725–1734
49. Lin, K., Lin, J., Wu, W.-I., Ballard, J., Lee, B. B., Gloor, S. L., Vigers, G. P. A., Morales, T. H., Friedman, L. S., Skelton, N., and Brandhuber, B. J. (2012) An ATP-site on-off switch that restricts phosphatase accessibility of Akt. *Sci. Signal.* **5**, ra37
50. Chan, T. O., Zhang, J., Rodeck, U., Pascal, J. M., Armen, R. S., Spring, M., Dumitru, C. D., Myers, V., Li, X., Cheung, J. Y., and Feldman, A. M. (2011) Resistance of Akt kinases to dephosphorylation through ATP-dependent conformational plasticity. *Proc. Natl. Acad. Sci. U. S. A.* **108**, E1120–E1127
51. Currie, R. A., Walker, K. S., Gray, A., Deak, M., Casamayor, A., Downes, C. P., Cohen, P., Alessi, D. R., and Lucocq, J. (1999) Role of phosphatidylinositol 3,4,5-trisphosphate in regulating the activity and localization of 3-phosphoinositide-dependent protein kinase-1. *Biochem. J.* **337**, 575–583
52. Schenck, A., Goto-Silva, L., Collinet, C., Rhinn, M., Giner, A., Habermann, B., Brand, M., and Zerial, M. (2008) The endosomal protein Appl1 mediates Akt substrate specificity and cell survival in vertebrate development. *Cell* **133**, 486–497
53. Braccini, L., Ciraolo, E., Campa, C. C., Perino, A., Longo, D. L., Tibolla, G., Pregnolato, M., Cao, Y., Tassone, B., Damilano, F., Laffargue, M., Calautti, E., Falasca, M., Norata, G. D., Backer, J. M., *et al.* (2015) PI3K-C2γ is a Rab5 effector selectively controlling endosomal Akt2 activation downstream of insulin signalling. *Nat. Commun.* **6**, 7400
54. Slagsvold, T., Marchese, A., Brech, A., and Stenmark, H. (2006) CISK attenuates degradation of the chemokine receptor CXCR4 via the ubiquitin ligase AIP4. *EMBO J.* **25**, 3738–3749
55. Carlton, J. G., and Cullen, P. J. (2005) Coincidence detection in phosphoinositide signaling. *Trends Cell Biol.* **15**, 540–547
56. Siess, K. M., and Leonard, T. A. (2019) Lipid-dependent Akt-ivity: Where, when, and how. *Biochem. Soc. Trans.* **47**, 897–908
57. Brunet, A., Park, J., Tran, H., Hu, L. S., Hemmings, B. A., and Greenberg, M. E. (2001) Protein kinase SGK mediates survival signals by phosphorylating the forkhead transcription factor FKHRL1 (FOXO3a). *Mol. Cell. Biol.* **21**, 952–965
58. Murray, J. T., Cummings, L. A., Bloomberg, G. B., and Cohen, P. (2005) Identification of different specificity requirements between SGK1 and PKBα. *FEBS Lett.* **579**, 991–994
59. Malik, N., Nirujogi, R. S., Peltier, J., Macartney, T., Wightman, M., Prescott, A. R., Gourlay, R., Trost, M., Alessi, D. R., and Karapetsas, A. (2019) Phosphoproteomics reveals that the hVPS34 regulated SGK3 kinase specifically phosphorylates endosomal proteins including Syntaxin-7, Syntaxin-12, RFIP4 and WDR44. *Biochem. J.* **476**, 741652
60. Tovell, H., Testa, A., Zhou, H., Shpiro, N., Crafter, C., Ciulli, A., and Alessi, D. R. (2019) Design and characterization of SGK3-PROTAC1, an isoform specific SGK3 kinase PROTAC degrader. *ACS Chem. Biol.* **14**, 2024–2034
61. Wu, W. I., Voegtli, W. C., Sturgis, H. L., Dizon, F. P., Vigers, G. P. A., and Brandhuber, B. J. (2010) Crystal structure of human AKT1 with an allosteric inhibitor reveals a new mode of kinase inhibition. *PLoS One* **5**, e12913
62. Lapierre, J. M., Eathiraj, S., Vensel, D., Liu, Y., Bull, C. O., Cornell-Kennon, S., Iimura, S., Kelleher, E. W., Kizer, D. E., Koerner, S.,

Makhija, S., Matsuda, A., Moussa, M., Namdev, N., Savage, R. E., *et al.* (2016) Discovery of 3-(3-(4-(1-Aminocyclobutyl)phenyl)-5-phenyl-3H-imidazo[4,5-b]pyridin-2-yl)pyridin-2-amine (ARQ 092): An orally bioavailable, selective, and potent allosteric AKT inhibitor. *J. Med. Chem.* **59**, 6455–6469

63. Weisner, J., Landel, I., Reintjes, C., Uhlenbrock, N., Trajkovic-Arsic, M., Dienstbier, N., Hardick, J., Ladigan, S., Lindemann, M., Smith, S., Quambusch, L., Scheinpflug, R., Depta, L., Gontla, R., Unger, A., *et al.* (2019) Preclinical efficacy of covalent-allosteric AKT inhibitor borussertib in combination with trametinib in KRAS-mutant pancreatic and colorectal cancer. *Cancer Res.* **79**, 2367–2378
64. Landel, I., Quambusch, L., Depta, L., and Rauh, D. (2020) Spotlight on AKT: Current therapeutic challenges. *ACS Med. Chem. Lett.* **11**, 225–227
65. Theile, C. S., Witte, M. D., Blom, A. E. M. M., Kundrat, L., Ploegh, H. L., and Guimaraes, C. P. (2013) Site-specific N-terminal labeling of proteins using sortase-mediated reactions. *Nat. Protoc.* **8**, 1800–1807
66. Bieniossek, C., Richmond, T. J., and Berger, I. (2008) MultiBac: Multigene baculovirus-based eukaryotic protein complex production. *Curr. Protoc. Protein Sci.* Chapter 5:Unit 5.20
67. Aricescu, A. R., Lu, W., and Jones, E. Y. (2006) A time- and cost-efficient system for high-level protein production in mammalian cells. *Acta Crystallogr. D Biol. Crystallogr.* **62**, 1243–1250
68. Sawa-Makarska, J., Baumann, V., Coudevylle, N., von Bülow, S., Nogellova, V., Abert, C., Schuschnig, M., Graef, M., Hummer, G., and Martens, S. (2020) Reconstitution of autophagosome nucleation defines Atg9 vesicles as seeds for membrane formation. *Science* **369**, eaaz7714
69. Rappsilber, J., Mann, M., and Ishihama, Y. (2007) Protocol for micro-purification, enrichment, pre-fractionation and storage of peptides for proteomics using StageTips. *Nat. Protoc.* **2**, 1896–1906
70. Cox, J., and Mann, M. (2008) MaxQuant enables high peptide identification rates, individualized p.p.b.-range mass accuracies and proteome-wide protein quantification. *Nat. Biotechnol.* **26**, 1367–1372
71. Perez-Riverol, Y., Csordas, A., Bai, J., Bernal-Llinares, M., Hewapathirana, S., Kundu, D. J., Inuganti, A., Griss, J., Mayer, G., Eisenacher, M., Pérez, E., Uszkoreit, J., Pfeuffer, J., Sachsenberg, T., Yilmaz, S., *et al.* (2019) The PRIDE database and related tools and resources in 2019: Improving support for quantification data. *Nucleic Acids Res.* **47**, D442–D450
72. Stariha, J. T. B., Hoffmann, R. M., Hamelin, D. J., and Burke, J. E. (2021) Probing protein-membrane interactions and dynamics using hydrogen-deuterium exchange mass spectrometry (HDX-MS). *Methods Mol. Biol.* **2263**, 465–485
73. Dobbs, J. M., Jenkins, M. L., and Burke, J. E. (2020) Escherichia coli and Sf9 contaminant databases to increase efficiency of tandem mass spectrometry peptide identification in structural mass spectrometry experiments. *J. Am. Soc. Mass Spectrom.* **31**, 2202–2209
74. Masson, G. R., Burke, J. E., Ahn, N. G., Anand, G. S., Borchers, C., Brier, S., Bou-Assaf, G. M., Engen, J. R., Englander, S. W., Faber, J., Garlish, R., Griffin, P. R., Gross, M. L., Guttman, M., Hamuro, Y., *et al.* (2019) Recommendations for performing, interpreting and reporting hydrogen deuterium exchange mass spectrometry (HDX-MS) experiments. *Nat. Methods* **16**, 595–602
75. Song, Y., Dimaio, F., Wang, R. Y. R., Kim, D., Miles, C., Brunette, T., Thompson, J., and Baker, D. (2013) High-resolution comparative modeling with RosettaCM. *Structure* **21**, 1735–1742